Hindawi Publishing Corporation
Journal of Aerodynamics
Volume 2014, Article ID 860637, 13 pages
http://dx.doi.org/10.1155/2014/860637

Research Article

Computational Aerodynamic Analysis of Offshore Upwind and Downwind Turbines

Qiuying Zhao, Chunhua Sheng, and Abdollah Afjeh

The University of Toledo, Toledo, OH 43606, USA

Correspondence should be addressed to Qiuying Zhao; qiuying.zhao@utoledo.edu

Received 10 July 2014; Accepted 30 September 2014; Published 29 October 2014

Academic Editor: Noor A. Ahmed

Aerodynamic interactions of the model NREL 5 MW offshore horizontal axis wind turbines (HAWT) are investigated using a high-fidelity computational fluid dynamics (CFD) analysis. Four wind turbine configurations are considered; three-bladed upwind and downwind and two-bladed upwind and downwind configurations, which operate at two different rotor speeds of 12.1 and 16 RPM. In the present study, both steady and unsteady aerodynamic loads, such as the rotor torque, blade hub bending moment, and base the tower bending moment of the tower, are evaluated in detail to provide overall assessment of different wind turbine configurations. Aerodynamic interactions between the rotor and tower are analyzed, including the rotor wake development downstream. The computational analysis provides insight into aerodynamic performance of the upwind and downwind, two- and three-bladed horizontal axis wind turbines.

1. Introduction

Wind turbines are designed to extract kinetic energy from the wind, usually to drive an electric generator. Almost all of the commercial wind turbines today are horizontal axis wind turbines (HAWT) [1, 2], meaning that the axis of rotation of the turbine rotor is horizontal. Two variations of this kind of wind turbine orientation are the upwind and downwind configurations. The upwind configuration has the rotor upwind of the tower, whereas the downwind configuration has the rotor downwind of the tower where the rotor rotates through the disturbed air produced by the tower's aerodynamic shadow. An upwind rotor generally requires stiffer blades, because the wind bends the rotor blades towards the tower. The requirements of more rigid blades for upwind turbines add to the rotor weight and thus increase the load applied to the bearing and the tower. In addition, the upwind turbines need a yaw control mechanism to keep the rotor facing the wind. Downwind turbines, on the other hand, do not typically need a yaw control mechanism if the rotor and nacelle have a suitable design to make the nacelle passively align with the wind. A significant advantage of the downwind turbine is that the rotor blades can be more flexible, decreasing the weight of the whole rotor system. The blades may bend at high wind speeds and reduce the load being passed to the tower. On the other hand, the disadvantage of the downwind turbine is the tower wake effect. The pressure fluctuations on the turbine as the rotor passes through the tower shadow may cause a higher fatigue load on the turbine and/or performance deterioration due to lower wind speed and possible dynamic stall on part of the blade.

When compared with the three-bladed design, the two-bladed wind turbine reduces the weight and cost by one rotor blade. Also, the three-bladed design requires more effort to transport assemble on site. In contrast, the two-bladed design is relatively easy to transport and may not require on-site assembly, thus lowering the cost. However, for the same rated power, the two-bladed turbines may increase the loading on individual rotor blade because of a larger chord, span, and/or rotational speed requirements. Due to the complexity of unsteady aerodynamics and structural response of large sized wind turbine blades, the wind turbine aeromechanic performance has been typically studied using a low-fidelity blade element momentum theory (BLMT) [3]. However, the wind turbine flow environment is challenging to model on

account of the dynamics of the rotating blades, the earth's boundary layer, and aerodynamic effects that occur when the rotor is out of alignment with the oncoming flow among other things. The boundary layer gradient together with a rotating rotor can lead to a yawing moment on the tower to a nonintuitive result. Effects such as flow separation and wake interaction with the tower make computational fluid dynamics (CFD) modeling and simulation of wind turbine flows an appropriate choice to investigate the unsteady aerodynamics.

Many experimental investigations of the aerodynamic influences for traditional wind turbine configurations are reported by researchers at the National Renewable Energy Laboratory (NREL) such as by Robinson et al. [2]. An experimental investigation of the aerodynamics and near wake characteristics of dual rotor wind turbines is also reported by Ozbay et al. [4]. In the area of computational investigations of wind turbine aerodynamics, Tongchitpakdee et al. [5] studied the turbulence models on the prediction of wind turbine aerodynamics. Duque et al. [6] investigated the performance of the NREL Phase VI wind turbine using both Navier-Stokes and comprehensive approaches. There are two major challenges in high-fidelity simulations of wind turbine flow fields. The first one is to accurately model the rotor flow characteristics such as laminar to turbulent flow transitions and flow separations or dynamic stalls. The second issue is to model the relative grid motion between the rotating rotor and tower to study their unsteady interactions. The actuator disk models [7], although effective in studying the general aerodynamics between the rotor and tower, are unable to capture the time-accurate unsteady phenomenon and thus impulsive loadings associated with each individual blade motion, which is critical in deterring the blade structural response and fatigue life of the whole wind turbine system. In the present study, high-fidelity numerical investigations are carried out using a computational fluid dynamics solver U^2NCLE [8], based on the NREL 5 MW reference wind turbine [1] for the three-bladed upwind and downwind, and two-bladed upwind and downwind configurations in order to obtain insight into offshore wind farm applications. The current investigations employ an advanced transitional modeling technology [9] coupled with the Spalart-Allmaras turbulence model [10] and an efficient sliding interface method [11] to address both physical and numerical modeling challenges faced in the wind turbine CFD simulations.

2. Computational Methods

2.1. Computational Fluid Dynamics Code: U^2NCLE. The unsteady Reynolds-averaged Navier-Stokes flow solver U^2NCLE [8] is used in the present study to compute the aerodynamic loads for all configurations of the NERL 5 MW wind turbine [1]. Unsteady time-accurate simulations are performed in the fixed reference frame where the main rotor is in relative motion with respect to the tower and nacelle. Implicit Newton iterations with Gauss-Seidel relaxation are used to march the unsteady solution. In the fixed frame, three to four Newton iterations with eight Gauss-Seidel relaxations

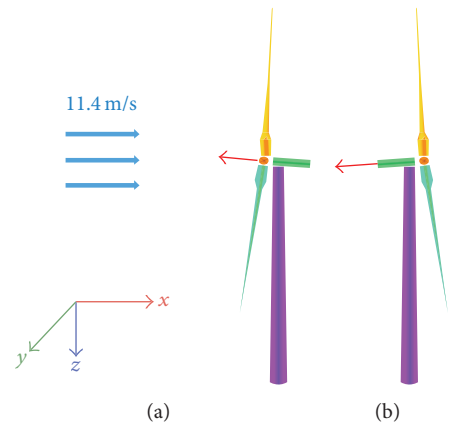

Figure 1: Upwind (a) and downwind (b) wind turbines.

are implemented with a prescribed time step corresponding to one-degree azimuthal rotation per time step. The 2nd-order spatially accurate Roe flux [12] is utilized. A directional derivative viscous method is used to calculate the viscous flux [13]. Characteristic variable boundary conditions [14] with specified free stream wind velocities are applied at the far field boundaries in the computational domain.

In order to capture the unsteady relative motion between the rotating rotor and the tower, an efficient unstructured grid sliding interface method [11, 15] is employed to render the relative motion between the rotor and the tower. The basic concept is to create a set of nested parent and child volume grids, where the motion in a child volume is considered as a combination of its own motion and that of its parent motion. This provides a flexible way to control the complex blade motions such as cyclic pitch and yaw control and to model the turbine-tower interactions in various upwind and downwind configurations. A unique advantage of the current method over the overset grid approach [6] is that no interpolation is required on the interface to exchange information between grids in relative motion because all the nodes are fully connected in the entire domain [11].

3. Geometry and Model Setup

3.1. NREL 5 MW Wind Turbine. The NREL offshore 5 MW baseline wind turbine [1] is a conventional three-bladed upwind variable-speed, variable blade-pitch-to-feather-controlled turbine. Figure 1 shows the sketch maps of this reference wind turbine in both upwind and downwind configurations. The bottom blade is pointing to the ground in the z direction, which is denoted as blade one at zero degree azimuth for both three-bladed and two-bladed cases. The wind turbine rotor blade has a radius of 63 meters. The rotor has 2.5-degree preconing angle and 5-degree shaft tilt angle. The wind turbine blade is composed of eight aerodynamic shapes including six airfoils and 2 cylinders with 13.3 degrees twist angle, as shown in Figure 2. The detailed distribution of the airfoils, associated chord lengths, and aero-twist angles along the blade span direction can be found in [1]. The tower

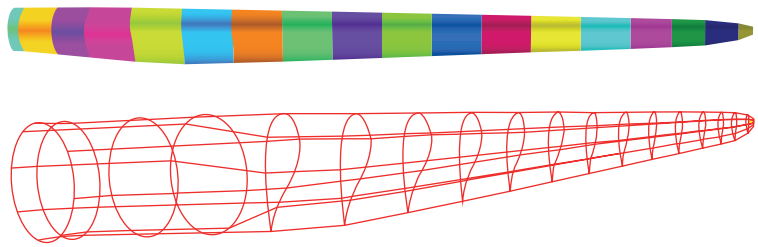

Figure 2: Wind turbine blade shape with sketch view.

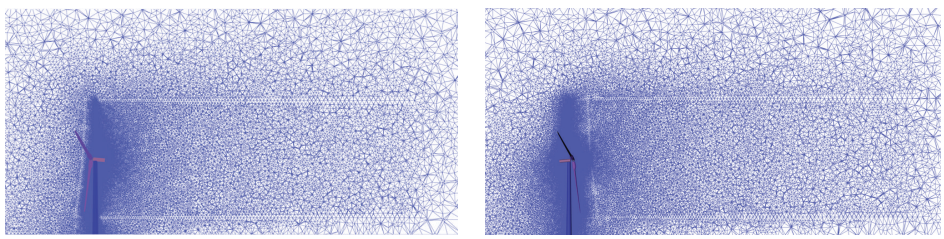

(a) (b)

Figure 3: Computational meshes of upwind (a) and (b) downwind configurations.

height is 87.6 meter, with the top and base diameter of 3.87 and 6 meters, respectively.

3.1.1. CFD Mesh and Flow Conditions. Four unstructured meshes corresponding to different wind turbine configurations were generated in the present study. Shown in Figure 3 are computational meshes for the upwind and downwind three-bladed turbines, which illustrate the grid density around the rotor and downwash regions. For all configurations, the same grid point spacing is used, with y^+ value of one applied to all viscous surfaces. The boundary growth ratio of two is used in the anisentropic volume grid regions. The volume grid sizes range from 8.56 (two-bladed) to 11.73 (three-bladed) million points for the combination of rotor, tower, hub, and nacelle. The blade surface mesh resolution near the tip region is shown in Figure 4. Regardless of the airfoil shape distribution, each blade is evenly separated into 36 sections based on the blade length from the hub to tip in order to provide sectional aerodynamic loads for a separate computational structural analysis [16]. The tower is also divided into 36 sections from the top to the ground base for the same purpose.

All computations were performed at the sea level atmosphere temperature of 15°C and pressure of 1.013×10^5 Pa. The rated wind speed of 11.4 m/s was chosen in all computations. The NREL 5 MW wind turbine has a diameter of 126 meters. Two rotational speeds of 12.1 RPM (rated) and 16 RPM were performed. The pitch angles are zero degree except negative 1.33 for the downwind two-bladed case with 16 PM at 75% span location from the center of rotation. The blade tip Mach number is 0.2346 for RPM 12.1 and 0.3102 for RPM 16. The corresponding Reynolds numbers are 689 million and 910 million based on the blade diameter and the rotor tip speed for RPM 12.1 and RPM 16, respectively.

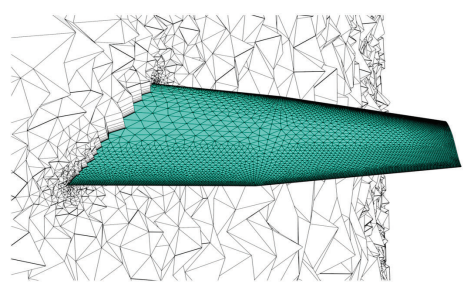

Figure 4: The blade surface grid resolution in the tip region.

4. Aerodynamic Analysis

In the wind turbine aerodynamic analysis, three important design parameters, the rotor orientation, the number of blades, and the rotor speed, are investigated in this study. Unsteady time-accurate simulations were performed using the high-fidelity CFD code U^2NCLE [8] on four wind turbine configurations, including the two-bladed upwind and downwind and the three-bladed upwind and downwind designs. All aerodynamic analyses were conducted at a rated wind speed 11.4 m/s [1]. A converged CFD solution for each case took about 10 rotor revolutions, or about 110–113 wall clock hours for the two-bladed cases and about 127–167 wall clock hours for the three-bladed cases, using 64 parallel processors. Computational simulations are performed at two sets of conditions: the same rotational speed of 12.1 RPM and the same rated power of 5 MW. Results are presented below in the order of rotor performance and blade hub moment, the tower base bending moment, and the wake impact to gain understanding of aerodynamic loadings and interactions in the wind turbine systems.

Table 1: Comparison of rotor power and torque.

Configuration	RPM	Power [MW]	Torque (mean) [N∗m] $*10^{-6}$	Torque (peak) [N∗m] $*10^{-6}$	(Peak − mean)/mean (%)
UW/3BLD	12.1	5.29	4.17	3.91	6.23
DW/3BLD	12.1	4.93	3.89	2.94	24.4
UW/2BLD	12.1	4.47	3.55	3.15	11.3
DW/2BLD	12.1	4.19	3.35	2.00	40.3
UW/2BLD	16	4.85	2.89	2.54	12.1
DW/2BLD	16	4.93	2.94	1.81	38.4

4.1. Rotor Performance. The rotor performance is investigated by evaluating the rotor power, torque, hub bending moment, and sectional loads. The computed rotor total power and mean and peak torque for different configurations are given in Table 1. The computed power at 12.1 RPM for the three-bladed upwind turbine is 5.29 MW, which is roughly 5.9% higher than the rated power of 5 MW. However, no direct comparison data are available between the reference wind turbine [1] and the CFD computed results. Considering the history of good correlations achieved for helicopter rotors using the current CFD code [17], it is believed that the wind turbine performance predicted in the current work is reliable, at least for the relative merit comparisons of different wind turbine configurations performed here. As expected, at the same rotor speed of 12.1 RPM, three-bladed turbines generated about 17% more power than the two-bladed turbines, since more rotor blades generally mean larger area to capture the wind and thus produce more power. The upwind turbines also produced slightly more power (about 7%) than the downwind turbines, due to the tower blockage effect that occurs in the downwind turbine configurations.

Perhaps more relevant comparisons should be made at the same rated power in order to develop relative merits among different wind turbine configurations. To match the rated power of 5 MW for the two-bladed turbines, the rotor speed has to be increased to 16 RPM. The pitch angle was slightly decreased by 1.33 degrees for the downwind case but remained the same for the upwind case. As shown in Table 1, the power of both three-bladed turbines at 12.1 RPM and two-bladed turbines at 16 RPM are close to the rated power of 5 MW, except for the three-bladed upwind case, which is slightly high.

The azimuthal distributions of the rotor total torque over one rotor revolution are shown in Figure 5, which provide the unsteady loads for different configurations. At the same rotor speed of 12 RPM, two-bladed turbines exhibited 17% smaller mean torque values than three-bladed turbines, which is the same as the rotor power generated. On the other side, because the torque is inversely proportional to the rotor speed at the rated power, the two-bladed wind turbines at 16 RPM had the smallest mean torque among all configurations, which is about 30% to 24% less than the three-bladed upwind and downwind turbines at 12.1 RPM, respectively.

Aside from the mean torque values, another important consideration in the wind turbine design is the unsteady loading. As illustrated in Figure 5, the downwind turbines experienced a larger unsteady variation than the upwind turbines, because of the tower shadow through which the downwind blades pass. Regardless the number of blades and the rotor speed, the peak-to-mean torque variation is about 6% to 12% for the upwind cases and 24% to 38% for the downwind cases, as shown in Table 1. The peak oscillation occurred more frequently in the three-bladed turbines than in the two-bladed cases, but the magnitude of the variation seemed to be larger in the two-bladed cases. These two factors, the frequency and the magnitude of the variation, are both important for the wind turbine structural and fatigue loads. The natural frequency of the downwind blade, with centrifugal stiffening included, should be different than the frequency at which the blade passes behind the tower. A structural dynamics simulation was performed in a separate paper to quantify the implication of the difference [16].

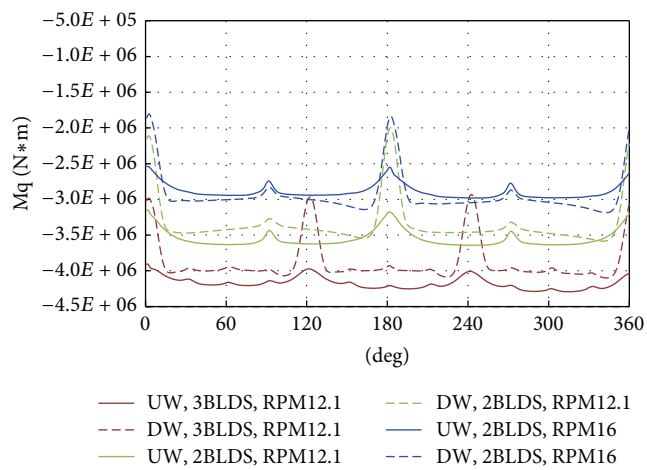

Figure 5: Rotor total torque variation over one rotor revolution.

The azimuth distributions of the sectional normal force and torque on a single blade are illustrated in Figures 6, 7, and 8. As shown in all figures, the peak values for both normal force and torque occurred at the same position, which is the blade and tower interaction. Negative torque values signify that the torque direction is opposite to the wind direction. The force and torque both gradually increase from the center of rotation to the tip until around 80% of the blade span and then decrease to the tip due to the reduction of the blade chord length in the tip region. The downwind rotor

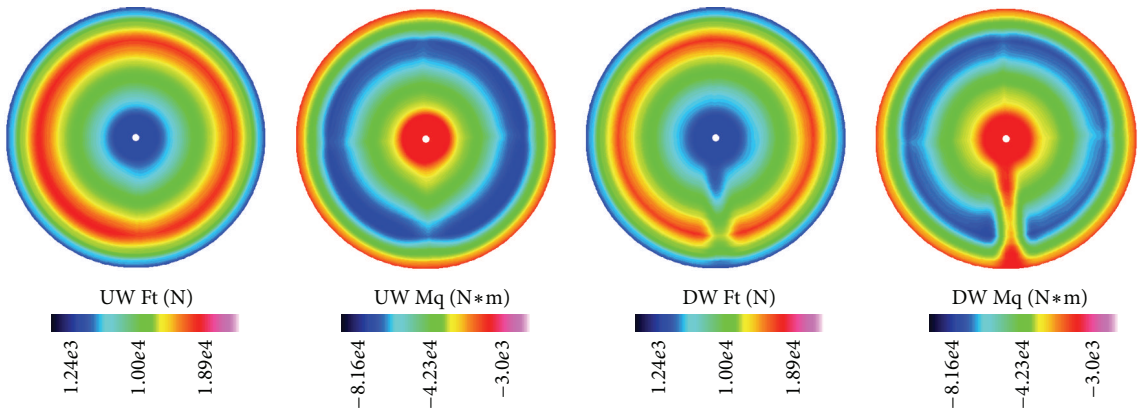

Figure 6: Three-bladed sectional normal force (Ft) and torque (Mq) distributions at 12.1 RPM.

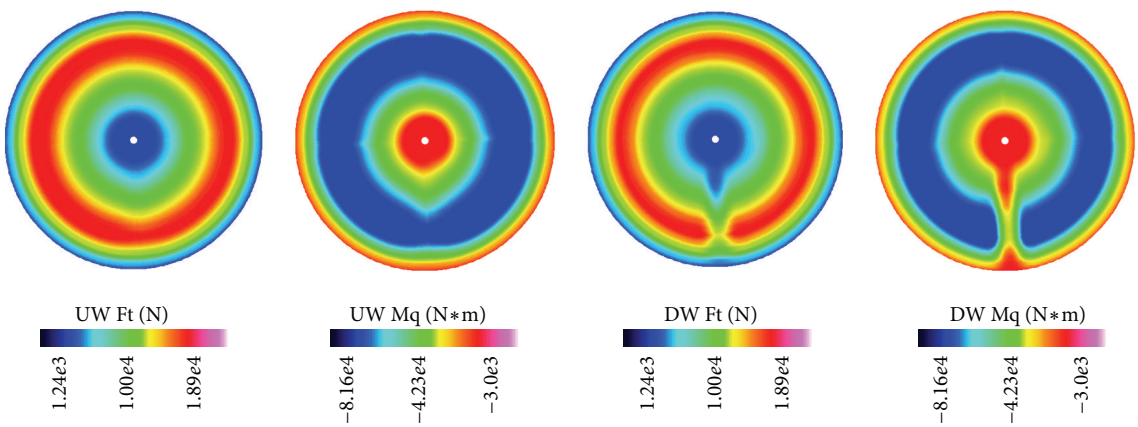

Figure 7: Two-bladed sectional normal force (Ft) and torque (Mq) distributions at 12.1 RPM.

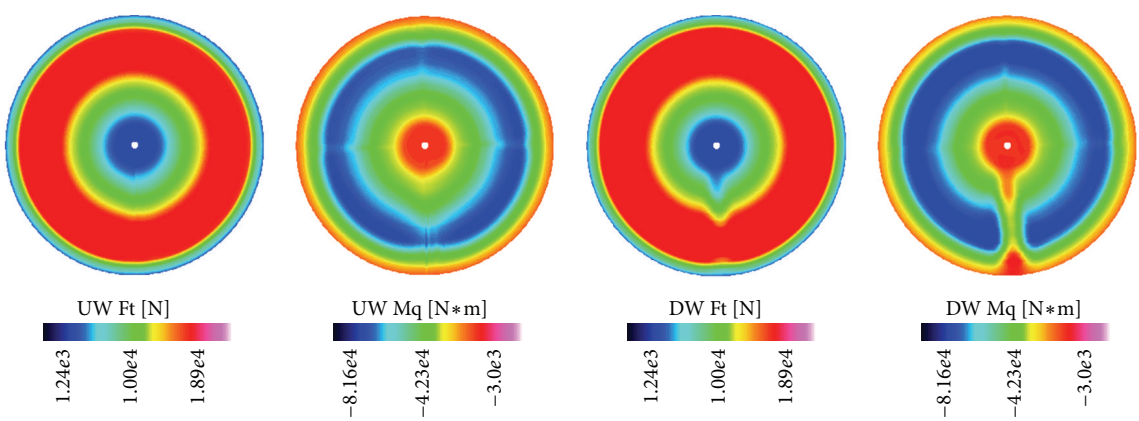

Figure 8: Two-bladed sectional normal force (Ft) and torque (Mq) distributions at 16 RPM.

showed a large reduction in normal forces and torques at the place where the rotor blade overlaps the tower, whereas the upwind case only a small amount of changes at the same location. Therefore, the upwind turbines exhibited more uniform force and torque distributions than the downwind turbines, meaning less unsteady loads.

The blade hub bending moment is a key consideration in the overall wind turbine design, because smaller bending moment means that less stiff design could be used to construct the rotor blades and reduce the overall costs. Both mean and peak bending moments are given in Table 2 for all wind turbine configurations. The dominating factor affecting the blade bending moment is the rotor speed. The two-bladed and three-bladed turbines had almost the same hub bending moment when operated at the same 12.1 RPM, although the two-bladed turbines had a slightly higher (9%) hub bending

Table 2: Comparison of blade hub bending moments.

Configurations	RPM	Hub moment (mean) [N∗m] $*10^{-7}$	Hub moment (peak) [N∗m] $*10^{-7}$	(Peak − mean)/mean (%)
UW/3BLD	12.1	1.32	1.26	4.5
DW/3BLD	12.1	1.25	0.88	29.6
UW/2BLD	12.1	1.43	1.35	5.6
DW/2BLD	12.1	1.35	0.93	31.1
UW/2BLD	16	1.94	1.85	4.6
DW/2BLD	16	2.12	1.67	21.2

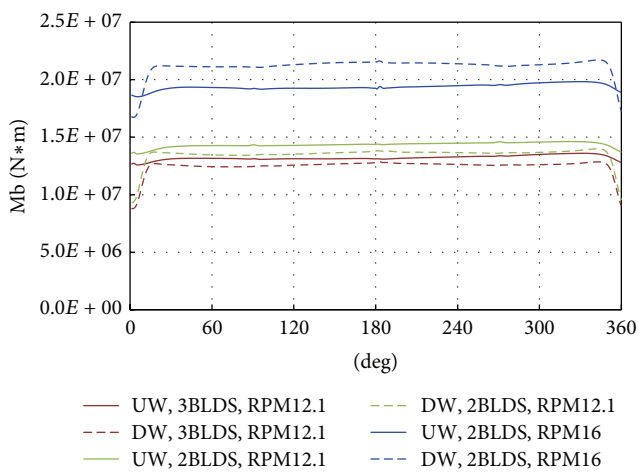

Figure 9: Blade hub bending moment variation over one blade revolution.

moment than the three-bladed counterparts. However, for the two-bladed turbines operating at 16 RPM, the blade hub bending moment was increased significantly by 47–70% in the upwind and downwind cases, respectively, comparing to the three-bladed turbines operating at 12.1 RPM. Increased blade bending moment means high structural loads to the wind turbine, which provides a major design challenge. A well-known solution for the two-bladed turbines was to attach a flexible structure with limited pivoting capability, called teeter hub [18], to eliminate or minimize the high structural loads resulting from the high bending moment.

Similar to the rotor torque analysis, equally important is the blade unsteady load that affects the wind turbine structural load and dynamic response. The azimuthal distributions of the blade bending moments for all configurations are shown in Figure 9, which illustrate the blade unsteady loading variations over one rotor revolution. Consistent with the previous analysis of the rotor torque, the downwind turbines produced a larger peak-to-mean variation in the blade bending moment than the upwind counterparts. This variation is from about 30% in the downwind turbines to about 5% in the upwind turbines. The structural dynamic analysis of these unsteady effects is performed in a separate paper, including the teetering joint for the two-bladed turbines, in order to quantify the impact of the blade bending moment on the structural load and dynamic response [16].

To develop improved understanding of the blade hub bending moments, it is necessary to evaluate the blade sectional bending moment distributions from the hub to tip at different azimuthal positions, which are shown in Figure 10. Evaluating the sectional bending moment helps identifying the weakest spot on the blade structure and/or adopting proper materials for different segments of the blade. For the same rotor speed of 12.1 RPM, the sectional bending moments are very close in all azimuth positions except for the position close to the tower, in which 25% reduction of the peak bending moment occurred in the downwind turbines. This was caused by the blockage effect of the tower in the downwind turbines. Nearly the same sectional bending moments were exhibited in the upwind and downwind turbines, but two-bladed turbines showed a slightly higher magnitude of the bending moments than the three-bladed turbines, which agrees with the previous analysis. For the same rated power, two-bladed turbines experienced much larger hub bending moments than the three-bladed turbines, from the hub to the tip at all azimuth locations. This is also consistent with total bending moment shown in Figure 9. For the two-bladed turbines, the sectional bending moments were maintained at the same level for all azimuths, except for the downwind turbine close to tower position. In general, two-bladed wind turbines experienced a slightly higher blade bending moment than the three-bladed counterparts at the same rotor speed 12.1 RPM but a significantly higher bending moment at the higher rotor speed of 16 RPM. In all cases, upwind turbines are less affected by the tower interaction, but a reduction of peak bending moment from 9% to 25% occurred in the downwind cases due to the blade and tower interaction.

In summary, the rotor performance was investigated for the upwind and downwind and three-bladed and two-bladed turbines at the same rotor RPM and the same rated power. The general finding here is that if the same rotor speed is maintained, changing the number of blades from three to two reduces the rotor total power and torque by around 17% in the upwind and downwind turbines. However, a slight higher torque is produced for the individual blade in the two-bladed turbines than in the three-bladed turbines, due to more uniform inflow in the two-bladed turbine operation. The blade hub bending moments are not significantly affected by different configurations, that is, three-bladed versus two-bladed or upwind versus downwind. However, to maintain the same rated power at a higher rotor RPM, two-bladed

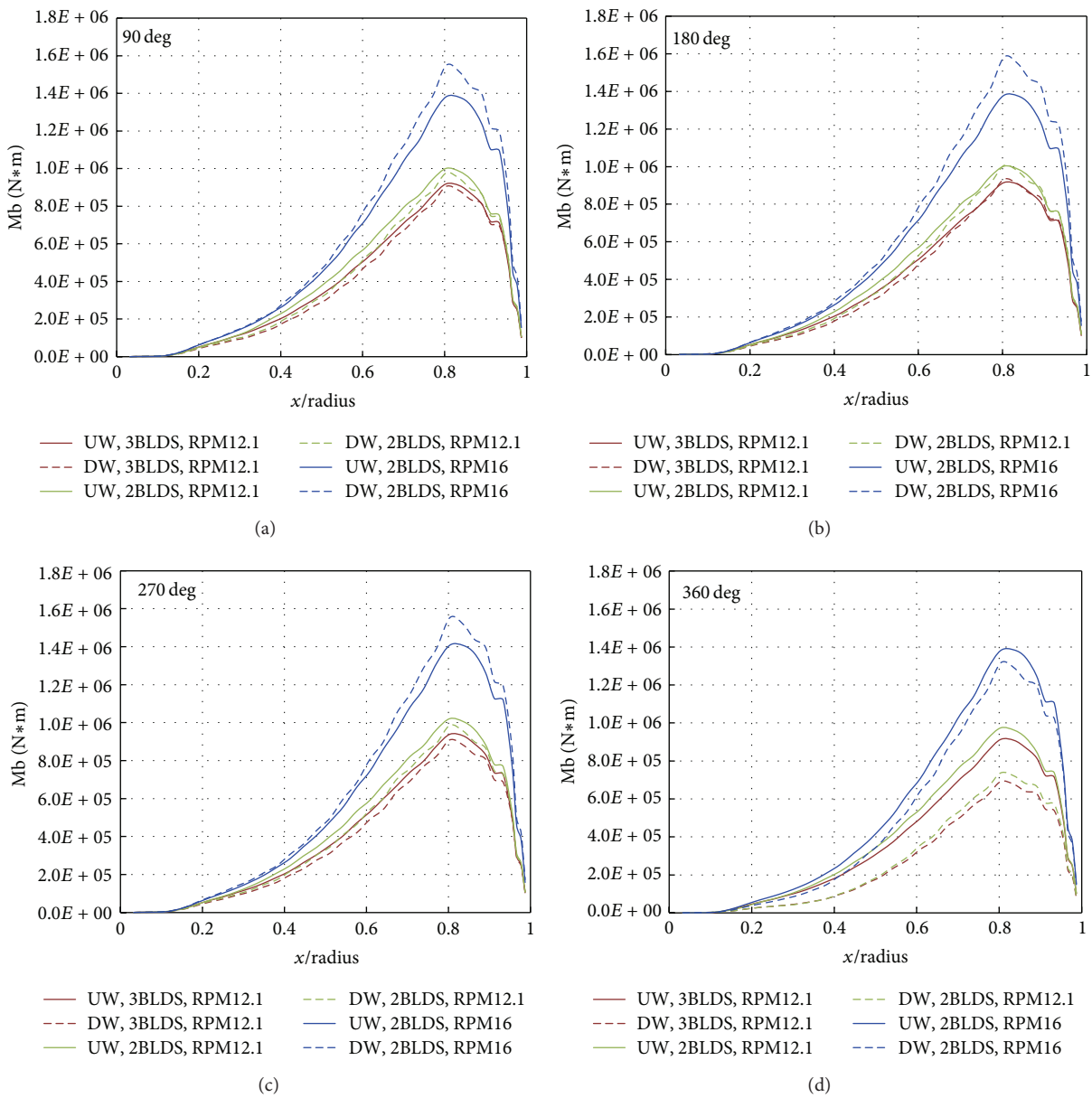

Figure 10: Sectional bending moment distributions at different azimuthal positions.

turbines have the blade hub bending moment increased significantly by 40% to 70% in the upwind and downwind cases, respectively. The increased blade bending moments in the two-bladed turbines should be further investigated using the structural analysis tool to evaluate the structural loads and dynamic responses to the wind turbine system.

4.2. Tower Loading. Due to the large size and weight of the wind turbine blades, the fatigue and structural load on the supporting tower is an important consideration in the wind turbine design. Rotor rotation and wind cause periodic loading on the tower. Table 3 compares the mean and peak values of the tower base bending moment, which includes forces acting on all rotor blades, hub, nacelle, and tower. Computational results indicated that the tower base moment is directly linked to the rotor power, because high rotor power means a high aerodynamic loading on the rotor blades, which is the dominating factor contributing to the tower base bending moment. For the same rotor speed at 12.1 RPM, the two-bladed turbines had less aerodynamic burden on the tower base than the three-bladed cases. Therefore, the mean base bending moments for the two-bladed turbines are about 27% less than those for the three-bladed counterparts. Without including the gravity effect, the downwind turbines also have about 4% less tower base bending moment than upwind turbines. This is also because of the tower blockage effect, which lessens the rotor bending effect on the tower. However, increasing the rotor speed to 16 RPM for the same level of power, the two-bladed turbines have nearly the same level of base bending moment of the tower as compared

Table 3: Comparison of the bending moment of the tower to the base center.

Wind turbine	RPM	Base moment (mean) [N∗m] $*10^{-7}$	Base moment (peak) [N∗m] $*10^{-7}$	(Mean − peak)/mean (%)
UW/3BLD	12.1	8.58	8.36	2.6
DW/3BLD	12.1	8.19	7.65	6.6
UW/2BLD	12.1	6.24	5.99	4.0
DW/2BLD	12.1	6.01	5.41	6.0
UW/2BLD	16	8.14	7.79	9.9
DW/2BLD	16	8.85	8.26	6.7

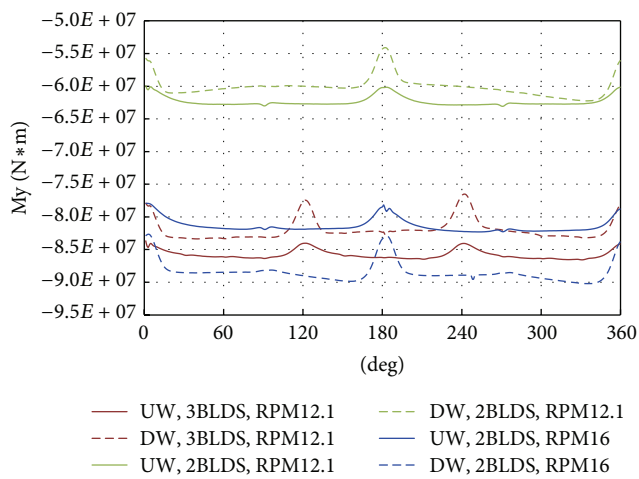

Figure 11: Comparison of total base bending moments of the tower.

with the three-bladed turbines at 12.1 RPM. In order words, no significant differences were found for the base bending moment of the tower in all wind turbine configurations considered, if the same rated power was maintained. However, since the above computational results were obtained based on pure aerodynamic forces without considering the weight of the rotor blades, the three-bladed turbines in reality may experience a higher base bending moment than what was predicted here. To quantify the effect of the rotor weight, a structural dynamic analysis has to be performed which includes the combination of all aerodynamic forces and structural masses of all wind turbine components [16].

The unsteady loads of the base bending moment of different wind turbines are shown in Figure 11. The overall pattern is very similar to the rotor torque distribution as shown in Figure 5. The frequency of the peak base bending moment closely correlates with the rotor torque in all configurations, but the magnitude of the peak to mean variations is smaller than the torque. Unlike the torque variations, where the percentage change can go as high as 40%, the maximum percentage change of the base bending moment in all cases is only 10%. At the rotor speed of 12.1 RPM, downwind turbines experienced slightly smaller base bending moment than the upwind cases. However, a larger base bending moment was found in the two-bladed downwind turbine at the rotor speed of 16 RPM, although the magnitude of the variation is smaller than that of the upwind two-bladed case.

The sectional base bending moments of the tower are investigated and compared for all wind turbines at different blade azimuth positions, which are shown in Figure 12. It should be mentioned that these sectional base moments only contained the contribution of the force acting on the tower and not contained the moment passed through by the rotor and nacelle to the base of the tower. In other words, the sectional moments shown in Figure 12 are only the dynamic component generated on the tower itself, and the actual base bending moment should also include the steady component of the rotor and nacelle moments to the tower base. Generally speaking, all downwind turbines experienced relatively stable sectional bending moments on the tower, especially at the rotor speed of 12.1 RPM. This was reflected by the same sign of the bending moment in the whole blade azimuthal positions. However, any sign change of the bending moment indicates an increased risk for the aerodynamic force to move the tower back and forth. The negative sign of the bending moment indicates that the wind force pushes the tower in the wind direction, and the positive sign means the moment direction against the wind. The switch of the moment direction was evident for all upwind turbine cases around the middle height location above the ground as the rotor blade passes through the tower. The peak aerodynamic bending moment values appeared around 80% of the height above the ground for the downwind turbines but occurred around 30–50% above the ground in the opposite direction to the wind for the upwind turbines. Although adding the steady moment contribution from the rotor and nacelle to the base bending moment will likely make the same negative sign of the sectional bending moment throughout the height of the tower, the sectional bending moments shown in Figure 12 illustrate the dynamic behavior of the tower, which directly affects the structural loads and responses of the tower. This observation reveals that pure aerodynamic loading for upwind designs tend to swing tower back and forth and thus increase the risk. The worst situation is the two-bladed upwind turbine operating at 16 RPM, which showed the biggest swing of the sectional base bending moment in all configurations.

The above analyses showed relative merits of the rotor and tower for different wind turbine designs, which may have contradicting features as desired. For example, the downwind turbines in general produced the smallest average and dynamic bending moments at the tower base but produced higher mean and maximum hub bending moments on the individual blades than the three-bladed turbines. In addition,

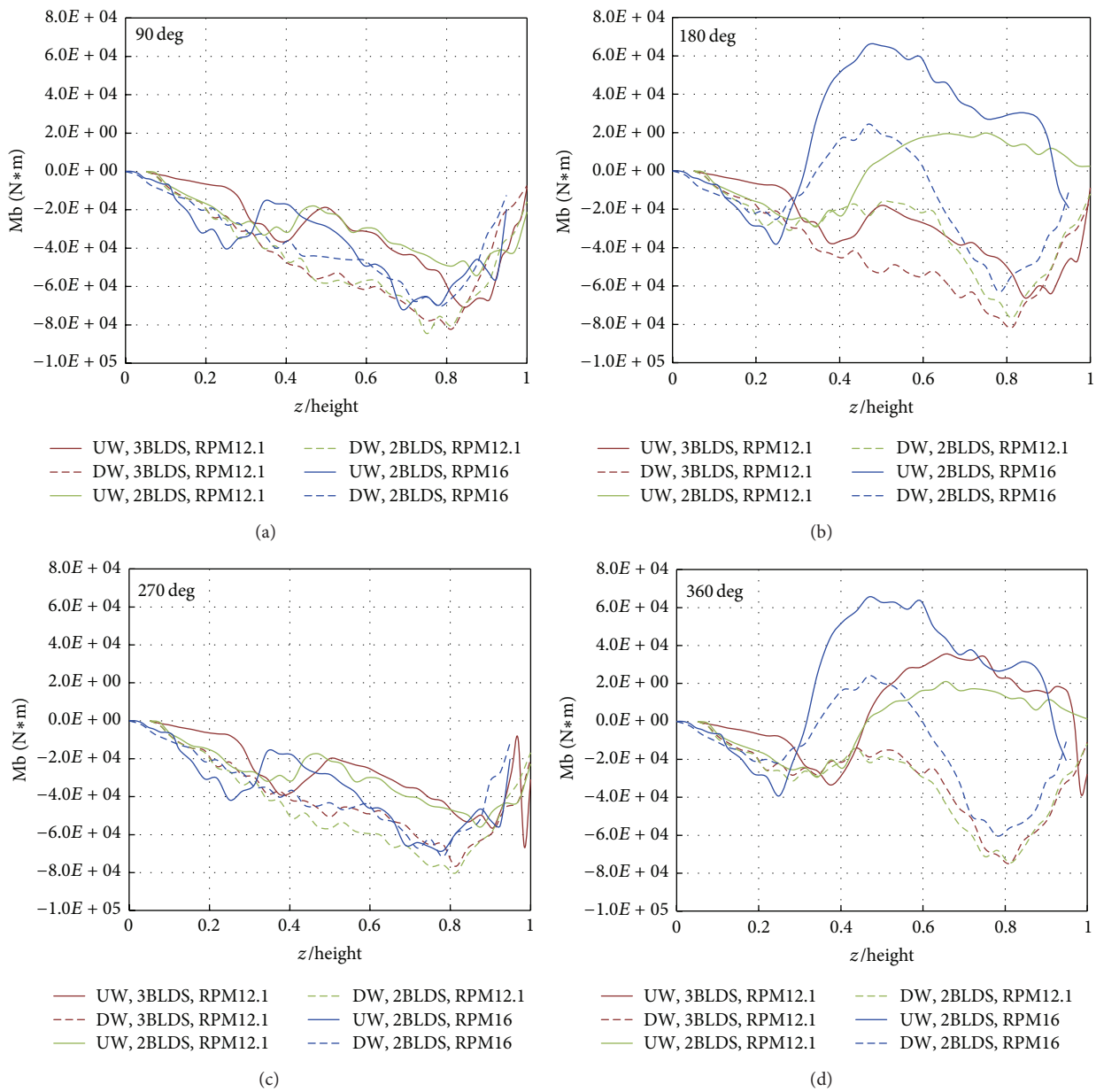

Figure 12: Sectional bending moments to the tower base center.

in the downwind turbines, the magnitude variation of the hub bending moments was significantly higher than that in the three-bladed upwind turbine, which can have adverse effects on the wind turbine structural and fatigue loads. To make the final determination on how important a given factor is for the fatigue and what impact that has on cost, a structural dynamic analysis needs to be performed.

4.3. Wake Impact. Because the wind turbine extracts kinetic energy from the wind, the air velocity decreases as air passes through the rotor. The wind turbine rotor also generates wake vortices lasting as far as several rotor diameters downstream, which will affect the inflow of the wind turbine placed in the near downstream, and its operation and performance. The wind speed gradually recovers to the undisturbed state when the wake effectively disappears because of mixing several rotor diameters away. In order to reduce the wake interference in a wind farm, the downstream wind turbine must be placed at a certain distance from the upstream one. Therefore, a correct estimation of the wind turbine spacing distance is essential to an optimal wind farm design.

The predicted instantaneous vorticity contours generated by upwind and downwind turbines as the blade one moves to the top position are exhibited in Figures 13, 14, and 15 in a vertical cutting plane through the rotor center along the wind direction. For the same blade pitch angle and rotor speed, stronger tip vortices were generated in the three-bladed turbines than that in the two-bladed turbines, consistent with

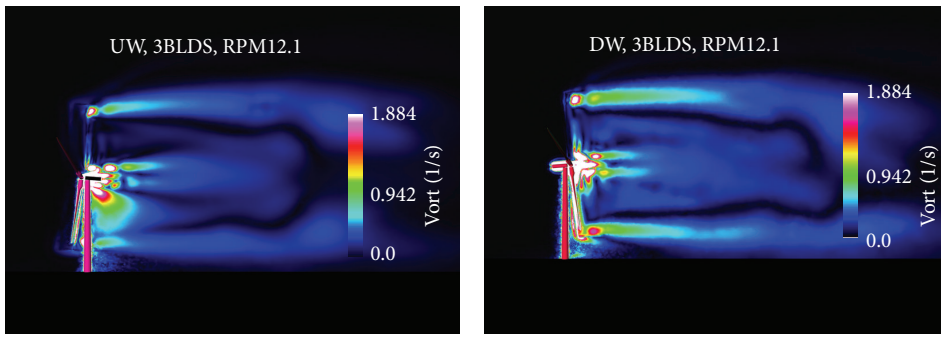

Figure 13: Instantaneous vorticity of three-bladed upwind and downwind turbines at 12.1 RPM.

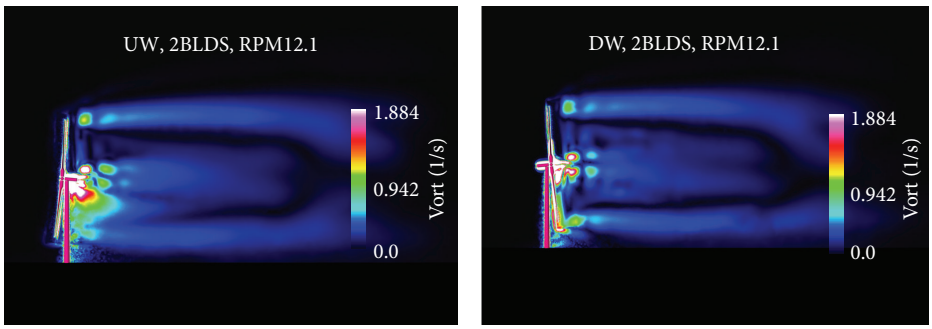

Figure 14: Instantaneous vorticity of two-bladed upwind and downwind turbines at 12.1 RPM.

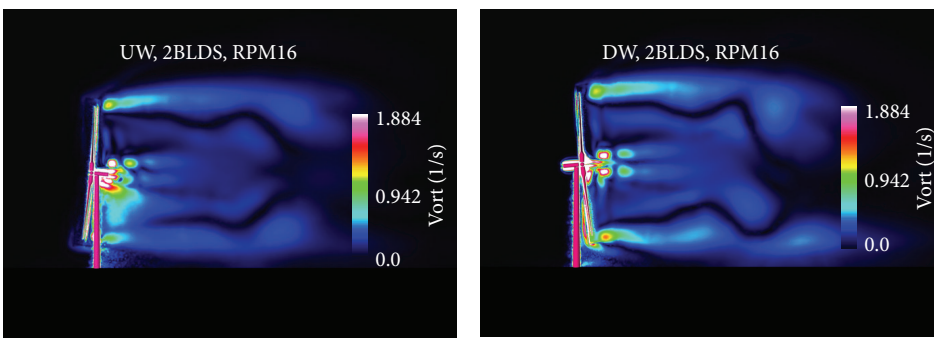

Figure 15: Instantaneous vorticity of two-bladed upwind and downwind turbines at 16 RPM.

more power being generated in the three-bladed wind turbines at the same rotor RPM. As the rotor speed increases to 16 RPM, stronger tip vortices were also generated in the two-bladed turbines. In general, the downwind turbines produced stronger rotor wakes than the upwind turbines, because the tower cut the wake generated by the upwind turbine at the lower portion of the rotor, and the wake-tower interaction helped to dissipate the wake more quickly compared with the downwind turbine case. The wake structure emanating from a wind turbine is of interest because it impacts turbine performance through distorted inflow velocity, which could negatively impact the performance of downstream turbines if they are placed too closely. The wake structures show expanding borders outward from the original radius, which is consistent with the windmill brake state, meaning that energy has been taken out of the flow.

The circumferentially averaged axial velocity variations along the vertical centerline parallel to the tower axis at several downstream locations up to five diameters downstream are shown in Figures 16, 17, and 18. The velocity approaches free stream wind velocity around about five rotor diameters downstream for wind turbines operating at 12.1 RPM. However, the wake velocity was recovered to the free stream much quicker at the higher rotor speed of 16 RPM, about three diameters downstream. Upwind cases revealed a more asymmetrical pattern due to the tower blockage effect, and thus downwind cases maintained a stronger wake than upwind cases at the same downwind distance. Larger variation of wake velocity magnitude was associated with the rotor power generated. In all these simulations, the 2nd order spatial accuracy scheme was used on modestly refined meshes in the rotor wake region, which may not

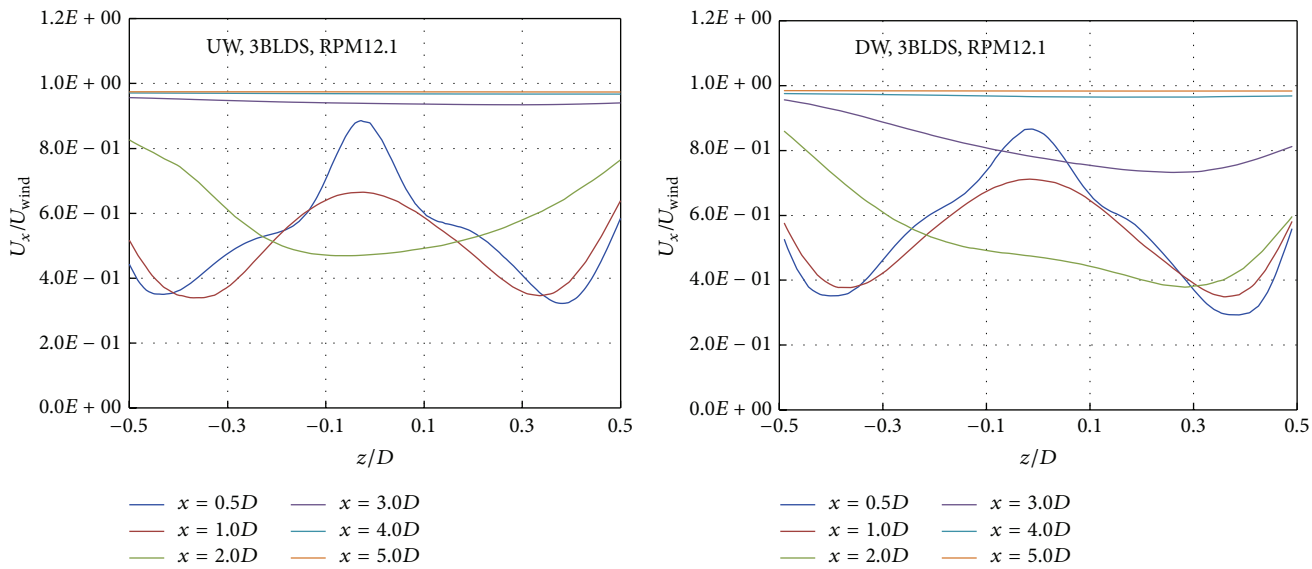

Figure 16: Downstream wake deficit of three-bladed upwind and downwind turbines at 12.1 RPM.

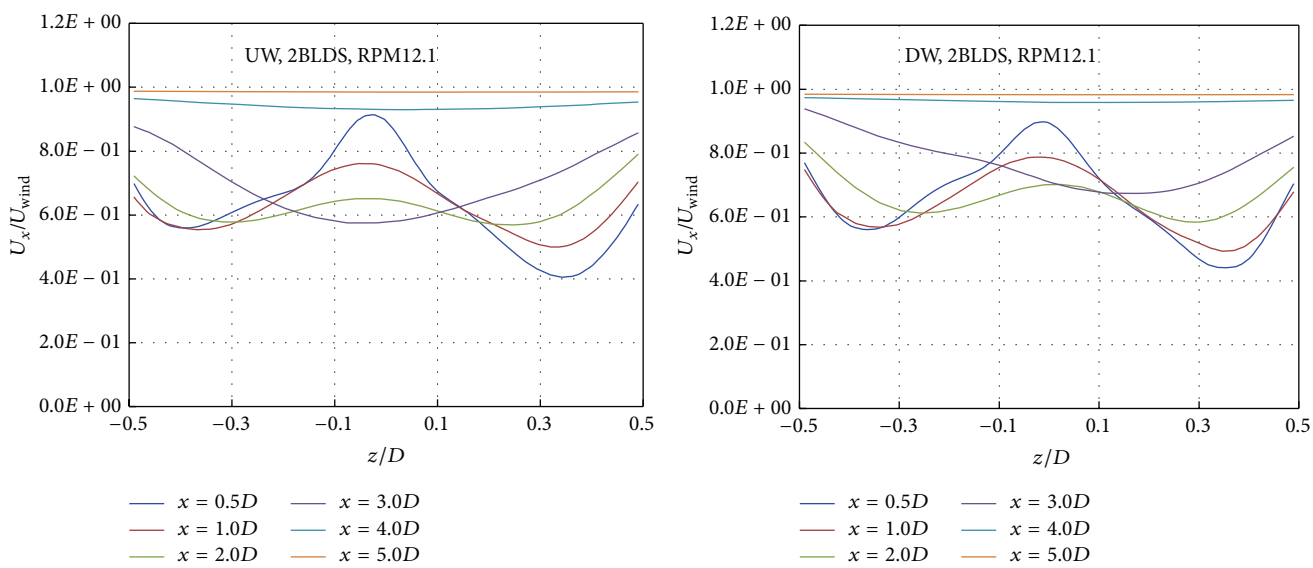

Figure 17: Downstream wake deficit of two-bladed upwind and downwind turbines at 12.1 RPM.

be good enough to maintain a longer effect of wakes due to nonphysical numerical dissipation. Nevertheless, these results provided the correct trends of the wake behavior for different configurations.

5. Conclusions

NREL 5 MW offshore wind turbine configurations were numerically investigated in the present study using a high-fidelity Navier-Stokes CFD code U^{2}NCLE, which included the three-bladed upwind and downwind turbines and two-bladed upwind and downwind turbines. Detailed aerodynamic analyses were performed on the rotor power and blade hub bending moment, the tower base bending moment, and the turbine wake flow. The relative merits of different wind turbine designs were discussed, as well as their implications on the structural loads and dynamic response. The following conclusions can be drawn from the current work.

(1) Both the blade number and rotor speed have the largest impact on the mean aerodynamic loading of the rotor power, blade hub bending moment, and base bending moment of the tower. The effect of the rotor orientation, that is, the upwind or downwind turbine, is secondary on the mean rotor aerodynamic loads but has a dominating impact on the unsteady loads of the wind turbine system.

(2) For the same rotor speed of 12.1 RPM and blade pitch angle, two-bladed wind turbines reduced the rotor

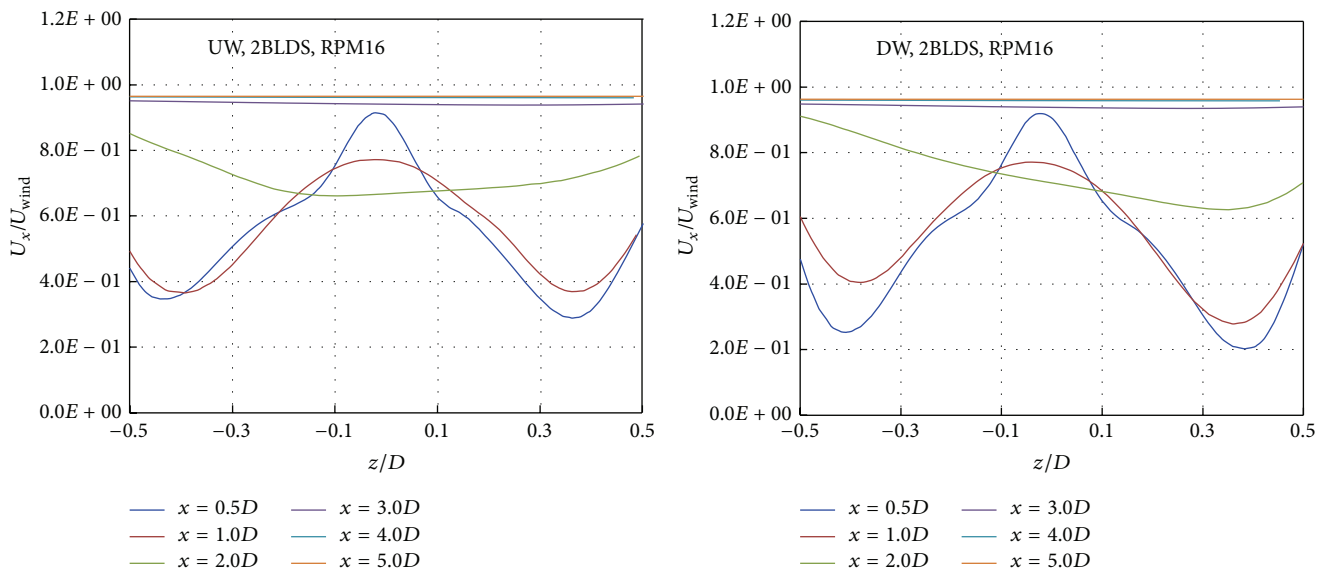

Figure 18: Downstream wake deficit of two-bladed upwind and downwind turbines at 16 RPM.

power by roughly 17% but increased the blade mean bending moment by 9% approximately, compared with the three-bladed counterparts. However, there was a 27% reduction of the base bending moment of the tower, due to the reduction of the power generated by two-bladed wind turbines.

(3) For two-bladed turbines operating at a rotor speed of 16 RPM or the rated power of 5 MW, there was a 17% reduction of the rotor torque compared with the three-bladed turbines operating at 12.1 RPM. However, the blade mean hub bending moment was increased significantly by 47% in the upwind case, and 70% in the downwind case, in comparison with the three-bladed counterparts, respectively. The base bending moment of the tower remained at the same level if the same rotor power was maintained.

(4) The unsteady loading was generally higher in the downwind turbines than in the upwind turbines. Excluding the weight, the two-bladed downwind turbine experienced the largest variation of the unsteady rotor torque, about 40% from the peak to the mean values, and about 21% to 30% of the blade bending moment variation comparing to roughly 5% variation in the upwind turbines. However, the tower unsteady load of the base bending moment was not significantly affected by the upwind and downwind turbine designs.

(5) Three-bladed wind turbines generated stronger rotor tip vortices than the two-bladed turbines did at the same rotor RPM. Two-bladed wind turbines generated stronger tip vortices at a higher rotor speed of 16 RPM, with the wake deficit recovered within a short distance downstream of the rotor. In general, a distance of five rotor diameters downstream is needed for the deficit velocity to recover to the uniform state.

Conflict of Interests

The authors declare that there is no conflict of interests regarding the publication of this paper.

Acknowledgment

The authors gratefully acknowledge the financial support for this project from the U.S. Department of Energy, Grant nos. DE-FG36-06GO86096 and DE-EE0003540.

References

[1] J. Jonkman, S. Butterfield, W. Musial, and G. Scott, "Definition of a 5-MW reference wind turbine for offshore system development," NREL Technical Report NREL/TP-500-38060, 2009.

[2] M. C. Robinson, M. M. Hand, D. A. Simms, and S. J. Schreck, "Horizontal axis wind turbine aerodynamics: three-dimensional, unsteady, and separated flow influences," in *Proceedings of the 3rd ASME/JSME Joint Fluids Energy Conference*, NREL/CP-500-26337, San Francisco, Calif, USA, 1999.

[3] T. Sant, *Improving BEM-based aerodynamic model in wind turbine design codes [Ph.D. thesis]*, University of Malta, 2007.

[4] A. Ozbay, W. Tian, and H. Hu, "An experimental investigation on the aerodynamics and near wake characteristics of dual-rotor wind turbines (DRWTs)," in *Proceedings of the 32nd ASME Wind Energy Symposium*, pp. 13–17, AIAA AciTech, National Harbor, Md, USA, January 2014.

[5] C. Tongchitpakdee, S. Benjanirat, and L. N. Sankar, "Numerical simulation of the aerodynamics of horizontal axis wind turbines under yawed flow conditions," in *Proceedings of the ASME Wind Energy Symposium at the 43rd AIAA Aerospace Sciences Meeting and Exhibit*, pp. 247–257, Reno, Nev, USA, January 2005.

[6] E. P. N. Duque, M. D. Burklund, and W. Johnson, "Navier-stokes and comprehensive analysis performance predictions of the nrel phase VI experiment," in *Proceedings of the 41st AIAA*

Aerospace Sciences Meeting and Exhibit (AIAA '03), Reno, Nev, USA, January 2003.

[7] R. Mikkelsen, *Actuator disc methods applied to wind turbines [Ph.D. thesis]*, Technical University of Denmark, 2003.

[8] C. Sheng, "A preconditioned method for rotating flows at arbitrary mach number," *Modelling and Simulation in Engineering*, vol. 2011, Article ID 537464, 17 pages, 2011.

[9] J. Wang and C. Sheng, "Validations of a local correlation-based transition model in an unstructured grid CFD solver," in *Proceedings of the 7th AIAA Theoretical Fluid Mechanics Conference*, Atlanta, Ga, USA, June 2014.

[10] P. Spalart and S. Allmaras, "A one-equation turbulence model for aerodynamic flows," AIAA Paper 92-0439, 1991.

[11] C. Sheng and J. C. Narramore, "Unsteady simulations of Bell-Agusta 609 rotor undergoing higher harmonic oscillation," *Journal of Aircraft*, vol. 45, no. 3, pp. 971–980, 2008.

[12] P. L. Roe, "Approximate Riemann solvers, parameter vectors, and difference schemes," *Journal of Computational Physics*, vol. 43, no. 2, pp. 357–372, 1981.

[13] D. Hyams, K. Sreenivas, C. Sheng, S. Nichols, R. Briley, and D. Whitfield, "An investigation of parallel implicit solution algorithms for incompressible flows on unstructured topologies," in *Proceedings of the 38th AIAA Aerospace Sciences Meeting*, AIAA-2000-0271, Reno, Nev, USA, January 2000.

[14] C. Sheng and X. Wang, "Characteristic variable boundary conditions for arbitrary mach number algorithm in rotating frame," AIAA Paper 2003-3076, 2003.

[15] C. Sheng and J. C. Narramore, "Computational simulation and analysis of bell boeing quad tiltrotor aero interaction," *Journal of the American Helicopter Society*, vol. 54, no. 4, Article ID 042002, 2009.

[16] C. Zhao, J. Ickes, C. Sheng, and A. Afjeh, "Numerical investigations of upwind and downwind NREL 5MW reference wind turbines using CFD and CSD," in *Proceedings of the American Helicopter Society 70th Annual Forum*, Momtreal, Canada, May 2014.

[17] C. Sheng, "Predictions of JVX rotor performance in hover and airplane mode using high-fidelity unstructured grid CFD solver," in *Proceedings of the American Helicopter Society 70th Annual Forum*, Montreal, Canada, 2014.

[18] E. De Vries, "Development of two-bladed offshore wind turbine," *Wind Stats Report*, vol. 24, no. 2, 2011.